1 Model evaluation for device C

1.1 Device information

The provided device is a single-poly transistor with a size of 1 * 5 μm^2 (drawn?) and a 121 contact configuration. Due to its complete isolation on all sides the transistor is expected to exhibit significant self-heating. The zero-bias internal base sheet resistance was specified to be 12 kΩ/sq.

The provided data consists of

- de-embedded S-parameters as a function of bias and frequency at the temperatures T=27C ; and with V_{CE} = const(various values);
- capacitance data (C_{BE} and C_{BC}) from LCR-meter measurements; substrate capacitance was provided as constant value (not from measurements).
- various DC bias data sets measured (on same device?) for different temperatures T/C=27, 75, 125 and with V_{BC} = const(various values)

1.2 Parameter extraction

The de-embedded S-parameter data (incl. bias information) were converted to y-parameters. In particular, data at a single frequency f = 0.687GHz were derived for the determination of f_T and an overall comparison of y-parameters over bias. A comparison of the DC data from S-parameter measurements and the DC data from DC measurements showed several percent difference between these data and a different shape of the $I_C(V_{BE})$ curves. This is shown in Fig. 1.2/1: at low current densities (e.g. V_{BE} = 0.8V) the collector current from DC data is visibly higher than the current from AC data, although its V_{CE} value (V_{CB}+V_{BE}=1.8V) is smaller than the AC V_{CE} value (2V); in addition, the slope is different, indicating that either the temperature was higher during the DC measurement or the measured device was different.

As a consequence, for parameter extraction *only the consistent data from S-parameter measurements ("AC" data) were employed*. The resulting model parameters were then applied to the data obtained from DC measurements ("DC" data), requiring modifications of a few parameters, while assuming the same junction capacitance and minority charge behavior (not available from "DC" data). Some of the parameter adjustments were related to the additional information available from "DC" data at lower current densities.

Initial parameters for junction capacitances (containing depletion and isolation components) were obtained from the provided measurements. Figs. 1.2/2 and 1.2/3 show the corresponding comparison between measured data (symbols) and model (lines). Note the extended scale by suppressing the y-axis origin. Some of the parameters had to be modified later due to differences to the values extracted from y-parameters (cf. Fig. 1.2/4 for C_{BC}) and in order to be able to model various physical effects (Early-effects, low-current transit time, transit frequency, avalanche breakdown) properly. C_{CS} from y-parameters turned out to be about twice the provided value (but indeed showed little bias dependence).

Open-collector data (cf. Fig. 1.2/5) was used in conjunction with a modified method to extract a realistic starting value for the emitter resistance r_E and its temperature coefficient. The value was slightly refined later, based on DC and y-parameter measurements. The non-linear shape of the curve is obvious, leading to a large error in r_E if simply a straight line would be attempted to fit to the curve.

Due to the isolation, there is no substrate transistor, and corresponding parameters were omitted.

Below, first the results obtained for the “AC” data set are shown, followed by results (and additional comments) for the “DC” data set. In many cases, the data are plotted vs. the (log of) collector current density I_C/A_E rather than vs. V_{BE}. The latter is of little interest and use for circuit design, and does not provide circuit design related information on the bias point. Note, that $V_{BE} \sim \log(I_C)$ for low current densities

.

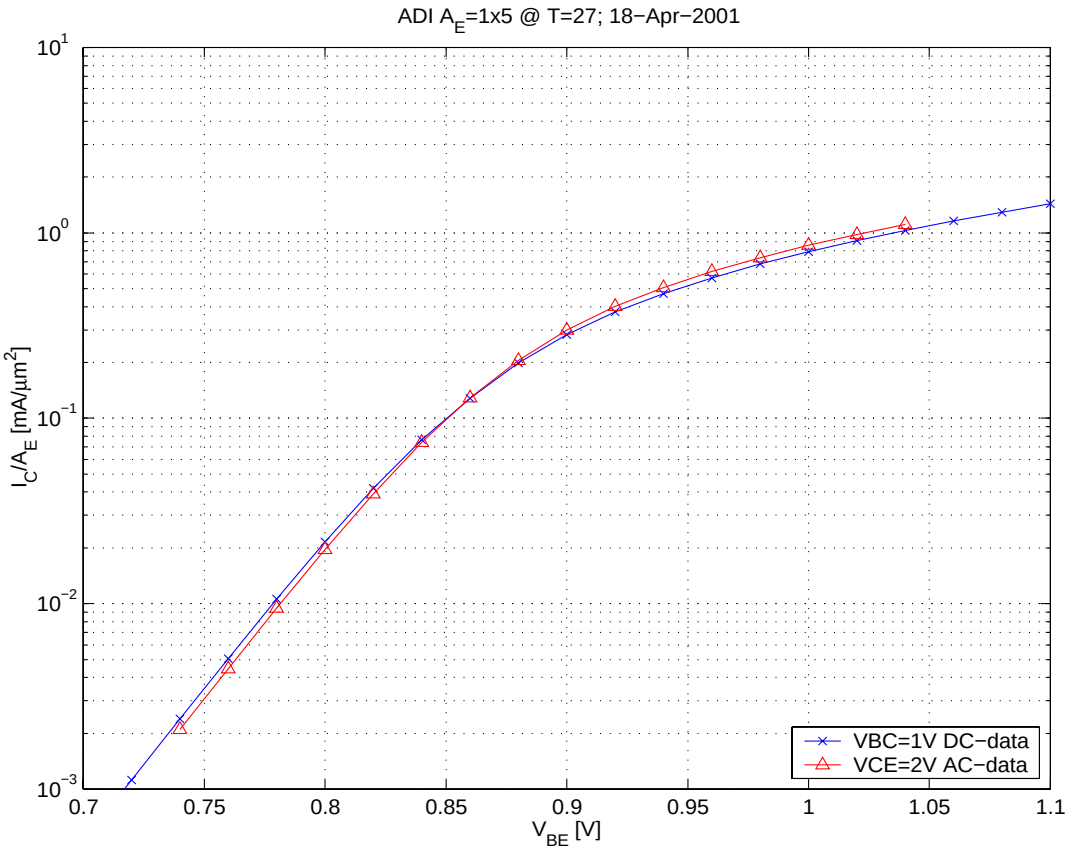

Fig. 1.2/1:Forward Gummel characteristics with data from different sources

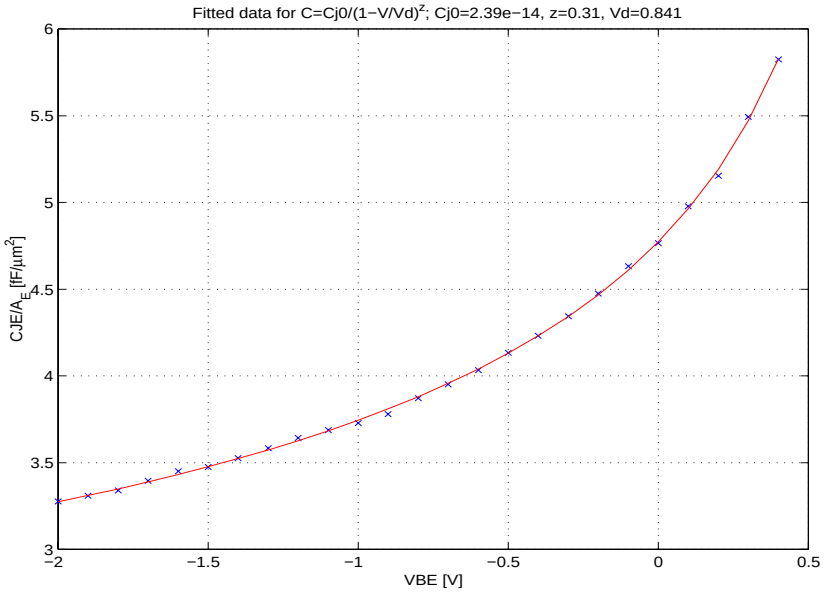

Fig. 1.2/2: Base-emitter capacitance vs. V_{BE}: measurement (symbols), HICUM (line).

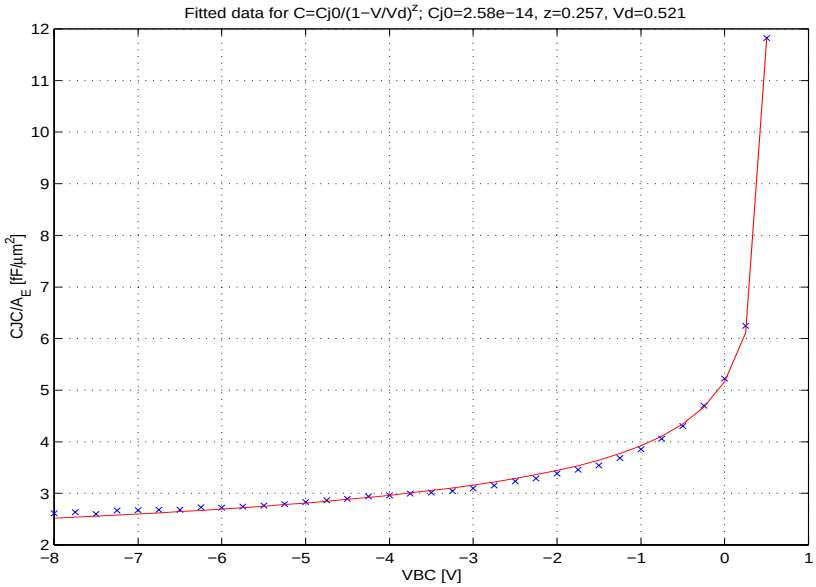

Fig. 1.2/3: Base-collector capacitance vs. V_{BC}: measurement (symbols), HICUM (line).

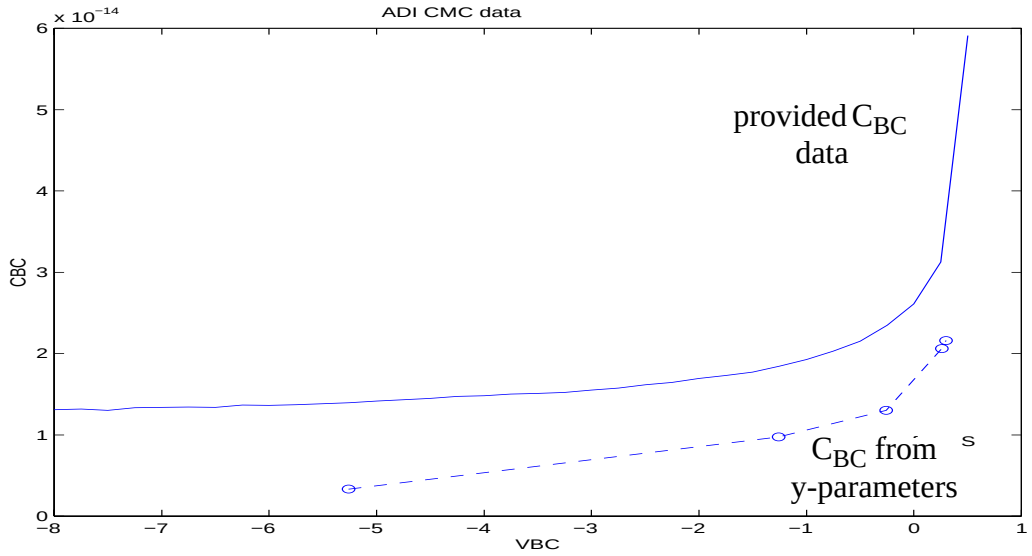

Fig. 1.2/4: Comparison of C_{BC} data (in [F]) from different measurement sources; V_{BC} in [V].

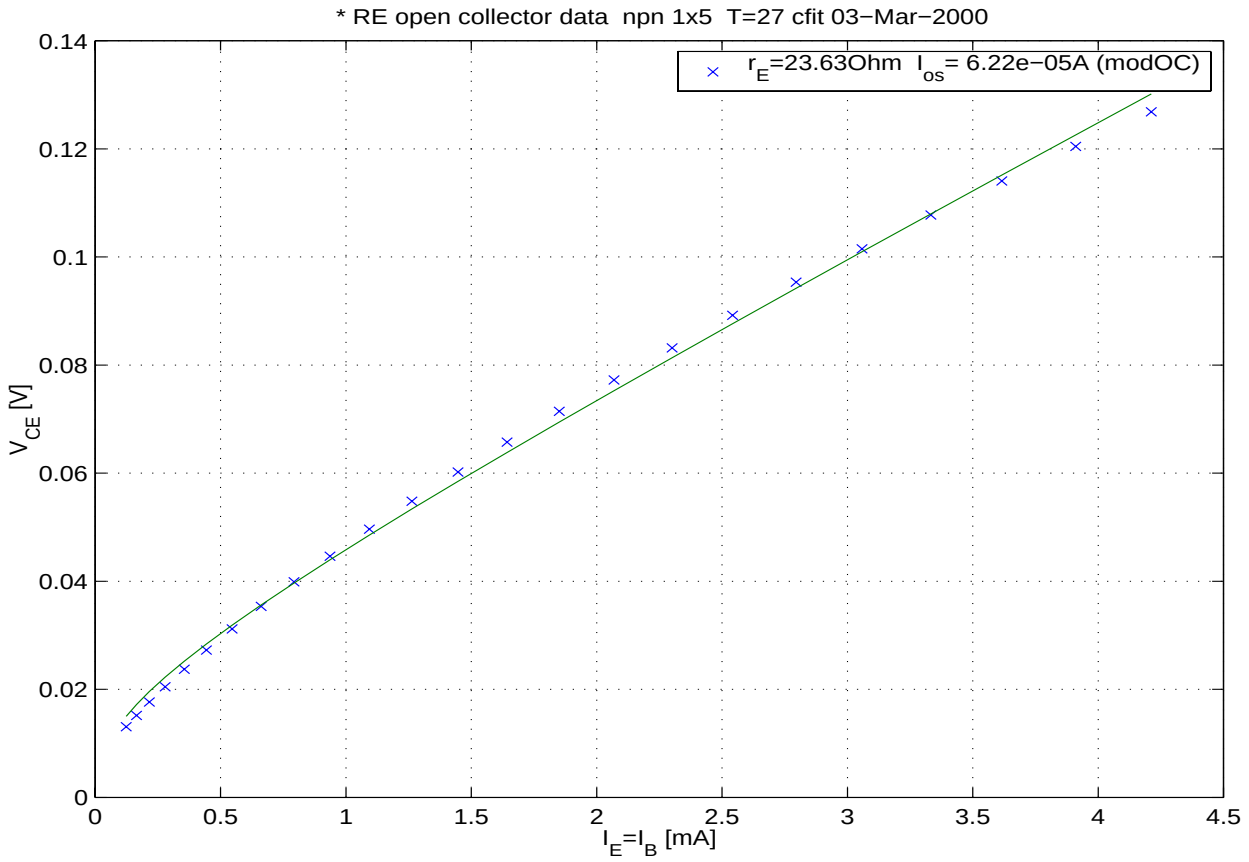

Fig. 1.2/5: Determination of r_E: modified open-collector measurement (symbols) and fit (line).

1.3 Results for the “AC” measurement data

Figures 1.3/1 and 1.3/2 contain a comparison of standard characteristics between model (solid lines) and measurements (symbols) within the interesting and available collector current density range. Good agreement is obtained up to fairly high current densities. Deviations can be caused by uncertainties in, e.g., (a) Q_{p0} (and geometry partitioning of depletion charges), (b) series resistances, (c) self heating and temperature coefficients and (d) geometry partitioning of the minority charge and associated current dependance (although the latter could be kept small due to the availability of f_T data). Information on I_B were not available in the respective “AC” data file. The transit frequency agrees quite well for all voltages and up to quite high current densities.

Fig. 1.3/3 shows the y-parameters as a function of collector current density at f = 0.687GHz and constant V_{CE} values. Fairly good agreement is obtained.

Figures 1.3/4 to 1.3/9 contain comparisons of frequency dependent y-parameters for selected bias points. In the first three figures, a set of curves was picked for V_{CE} = 0.5V, which is an extreme case, especially at high current densities: fairly good results are obtained even for current densities at and beyond those where f_T peaks. In the last three figures, the curves were selected for the highest available voltage V_{CE}=6V in order to demonstrate the capability of HICUM to cover a large bias range without loss of accuracy. For both voltages, the agreement at the bias points with lower current densities (Figs. 1.3/4 and 1.3/7) is also quite good. At frequencies below 0.1GHz, the measurement uncertainty does not seem to allow a clear conclusion. For the transistor provided, a simple substrate resistance seems to give reasonable agreement for modeling the substrate coupling in y_{22}.

In summary, the combination of parameter values found during fitting (cf. Fig. 1.3/10) describe the operating regions of interest reasonably well at least up to peak f_T, but can still be improved by both an independent determination of, e.g., series resistances and geometry effects, and the availability of additional *consistent* measured data for the capacitances. Alternatively, optimization (which was not used for extracting here) is also likely to improve the agreement.

Note that (a) f_T peaks - depending on V_{CE} - between J_C values of 0.07 and 0.2 mA/μm^2; (b) operation beyond peak f_T is of interest only for circuits switching at high-speed, in which the dynamic base current is much larger than the DC base current, making accurate DC base current modeling irrelevant compared to accurate modeling of charges which is reflected by f_T and in some cases also by, e.g., f_{max}.

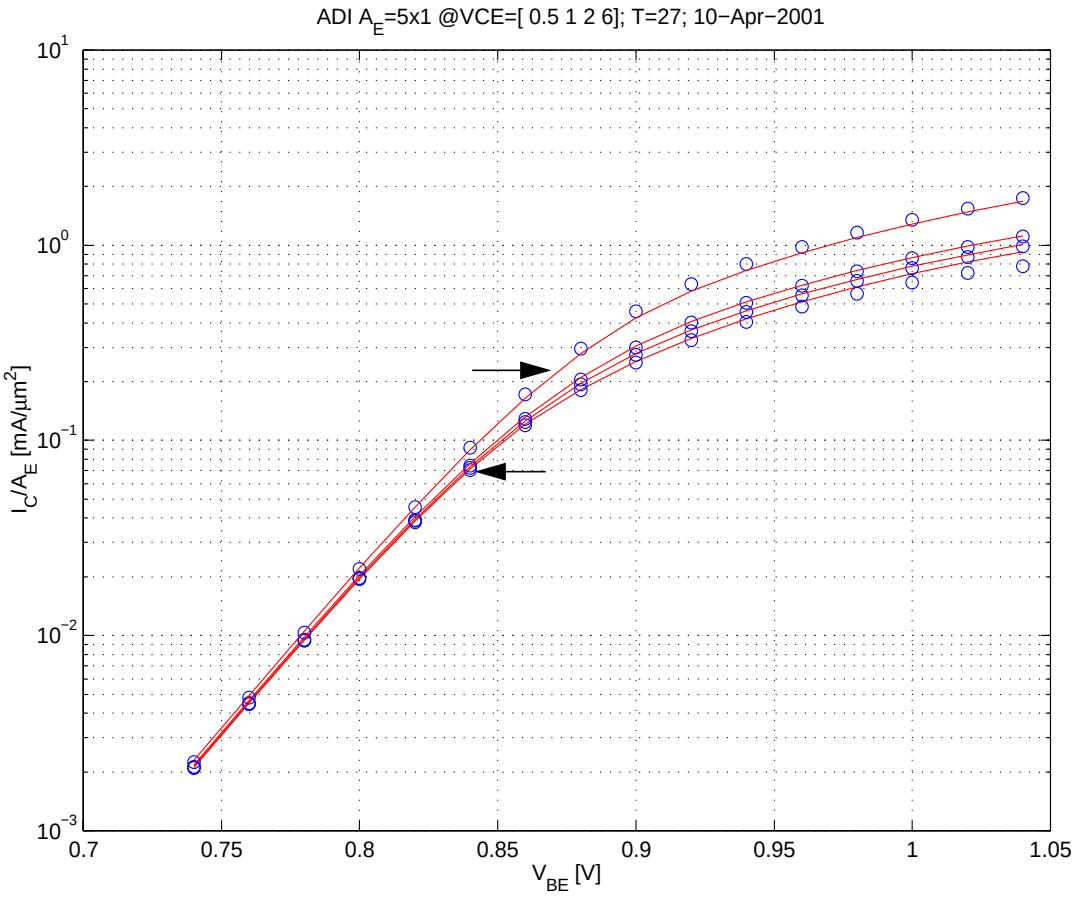

Fig. 1.3/1: Collector current density vs. V_{BE} for V_{CE}/V = 0.5, 1, 2, 6; T=27C. Data source: AC measurements.
The arrows indicate peak f_T for the lowest and highest V_{CE} value.

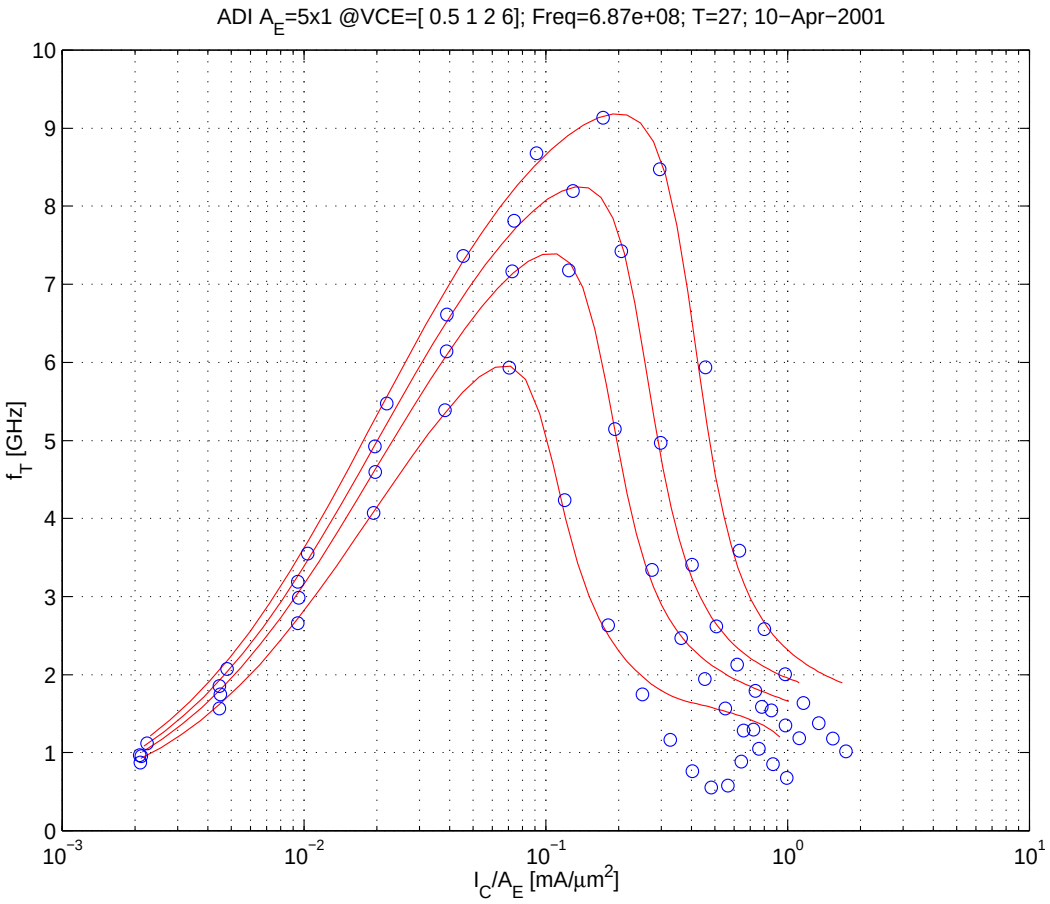

Fig. 1.3/2: Transit frequency vs. collector current density for V_{CE}/V = 0.5, 1, 2, 6; T=27C.

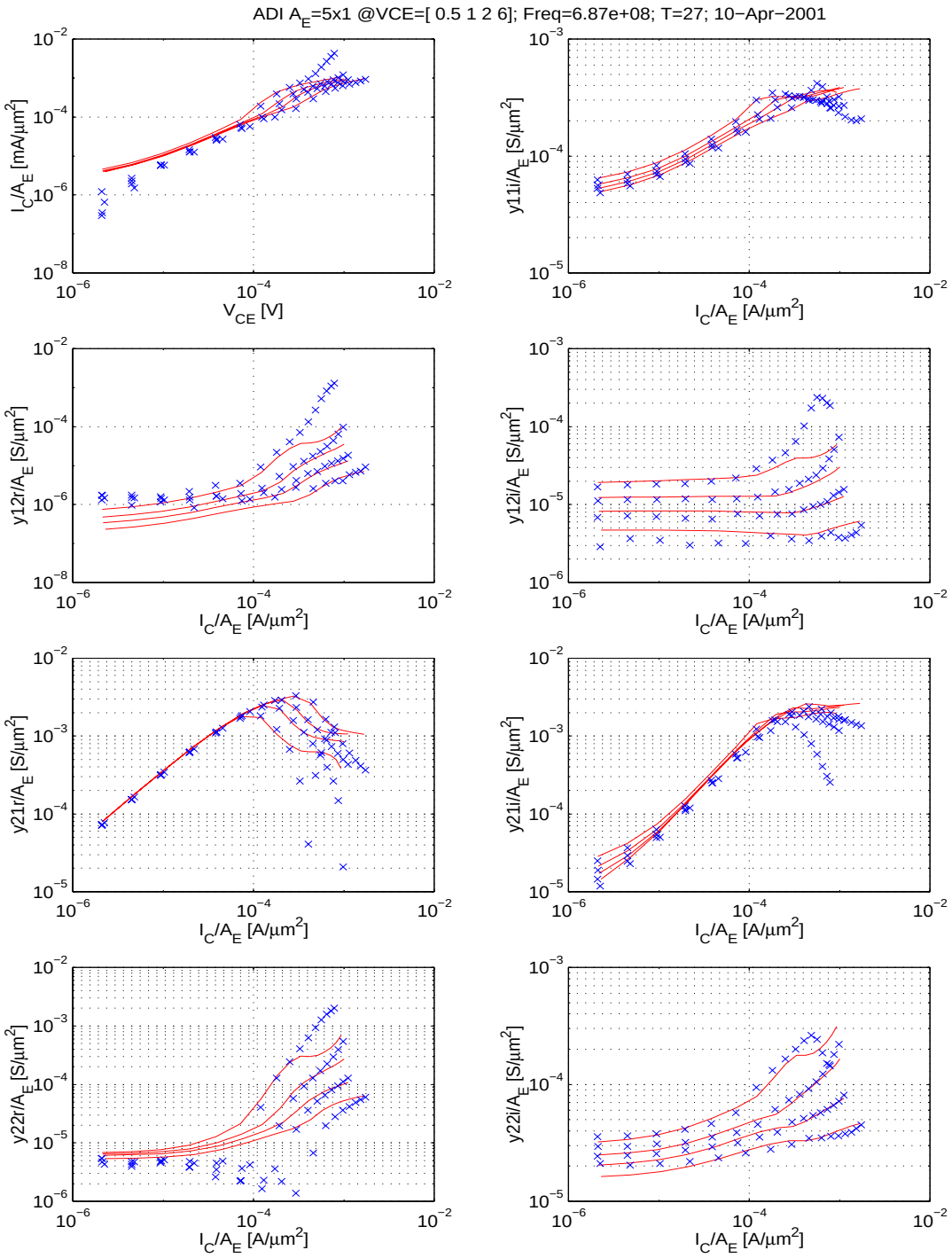

Fig. 1.3/3: Y-parameters vs. collector current density at f=0.687GHz; V_{CE}/V = 0.5, 1, 2, 6; T=27C.

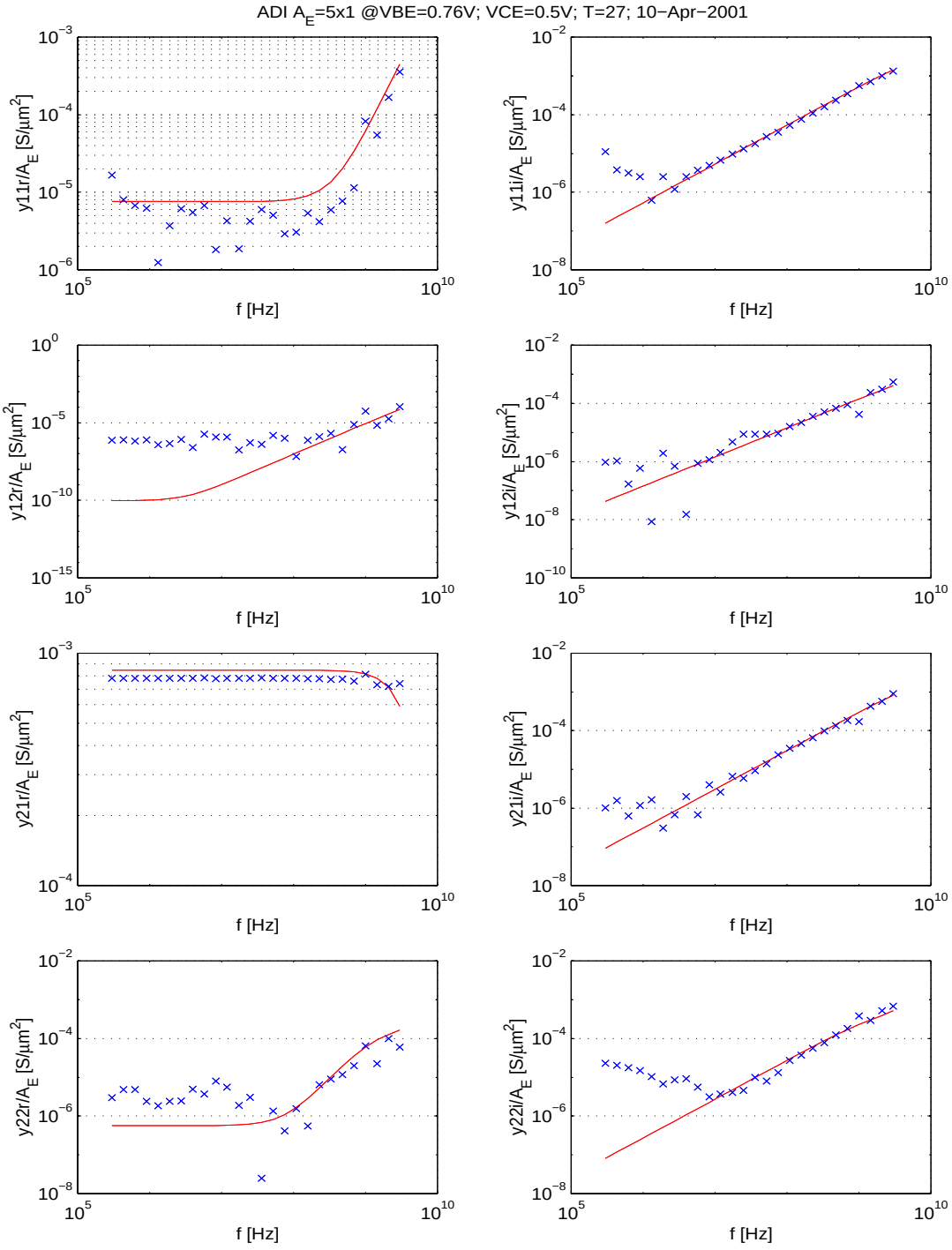

Fig. 1.3/4: Frequency dependent y-parameters at V_{CE} = 0.5V and I_C/A_E below peak f_T.

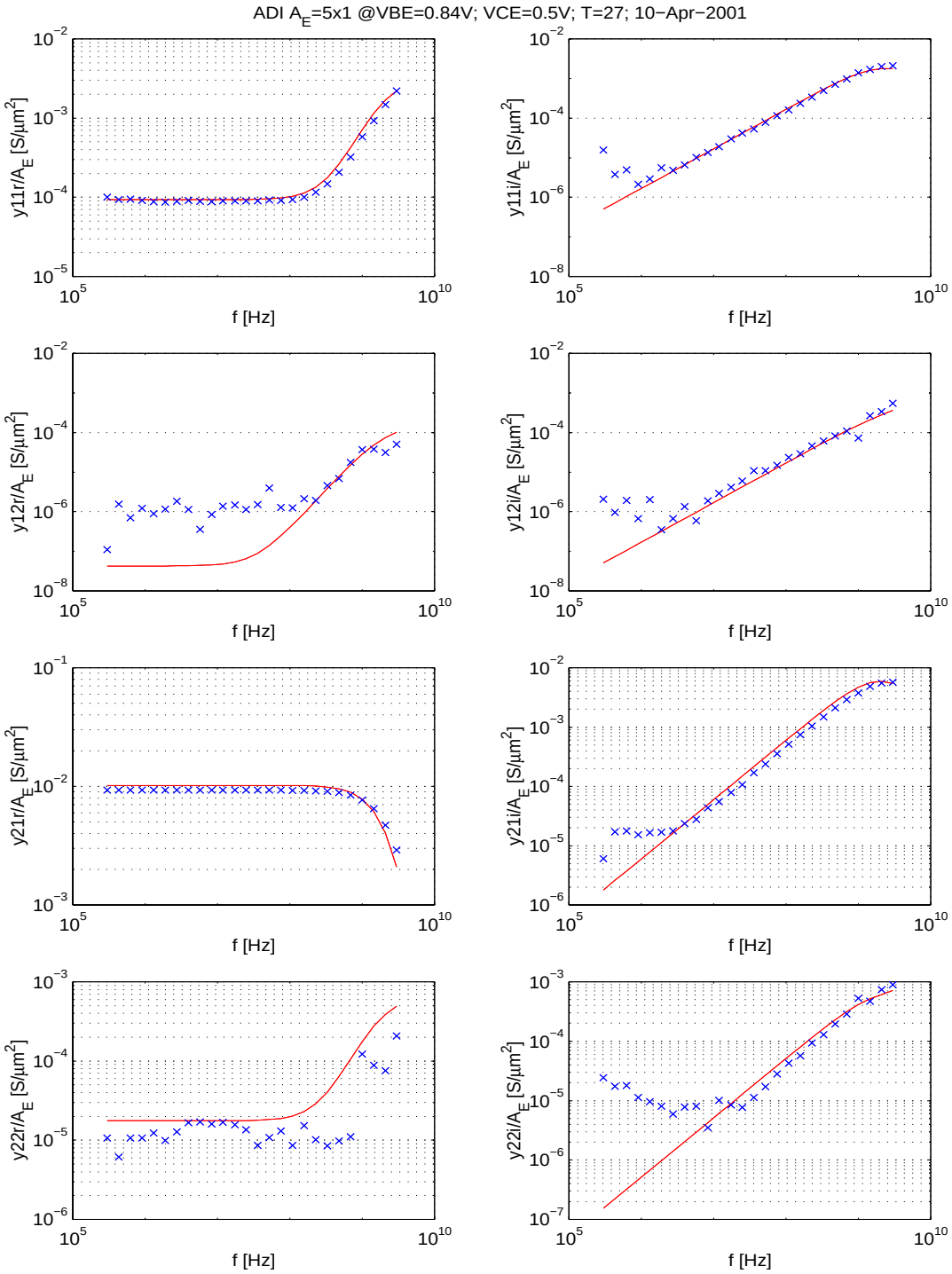

Fig. 1.3/5: Frequency dependent y-parameters at V_{CE} = 0.5V and I_C/A_E at peak f_T.

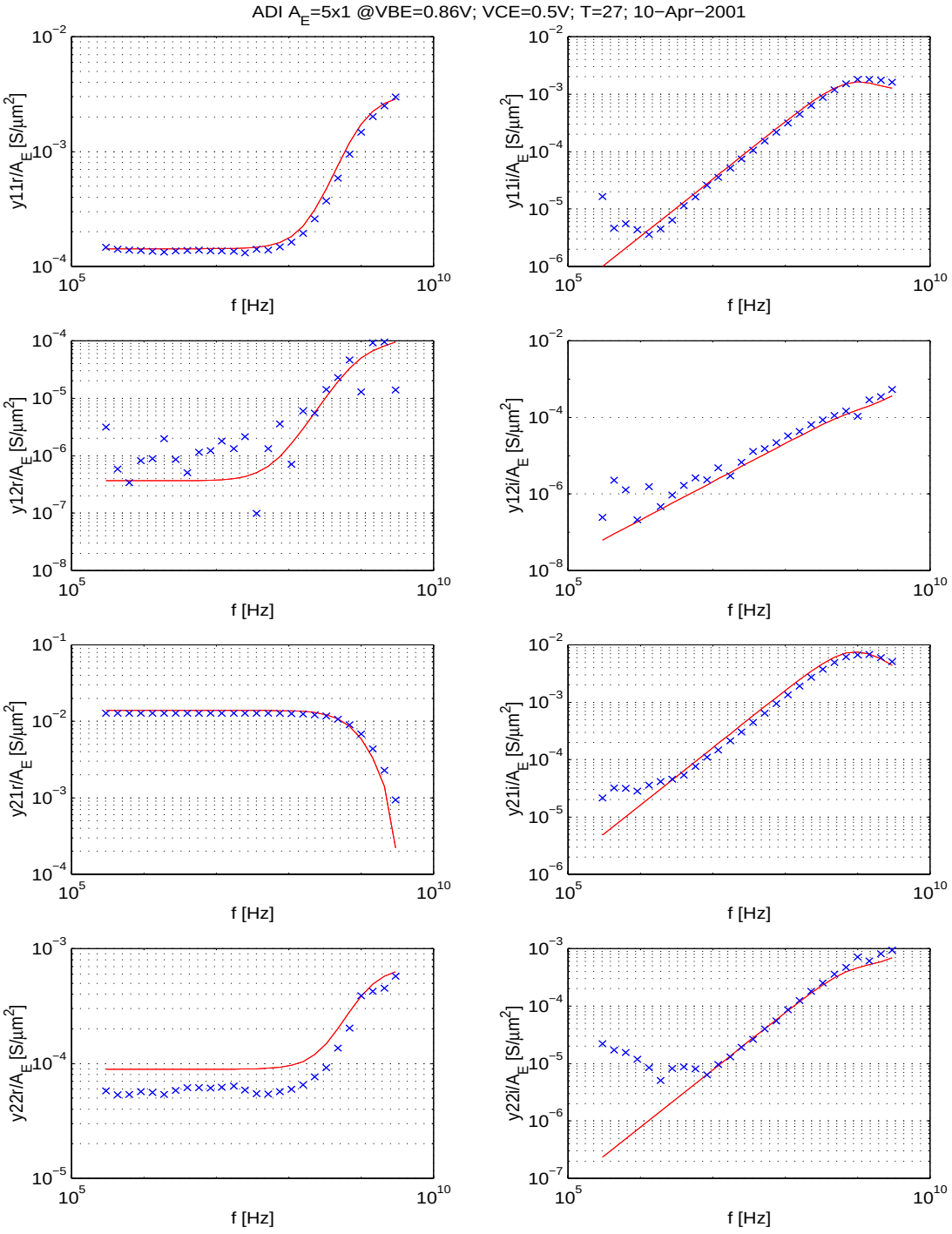

Fig. 1.3/6: Frequency dependent y-parameters at V_{CE} = 0.5V and I_C/A_E beyond peak f_T.

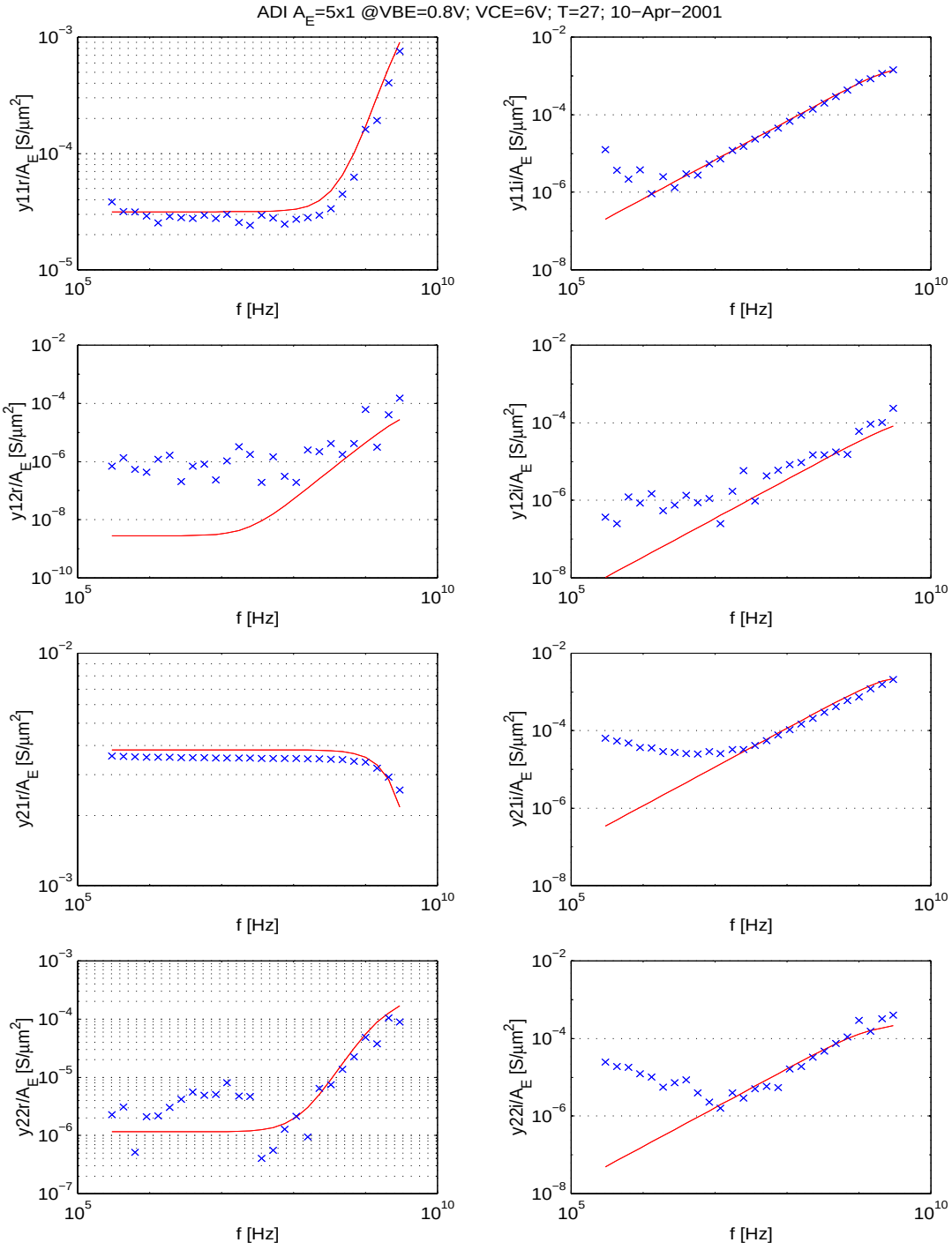

Fig. 1.3/7: Frequency dependent y-parameters at V_{CE} = 6V and I_C/A_E below peak f_T.

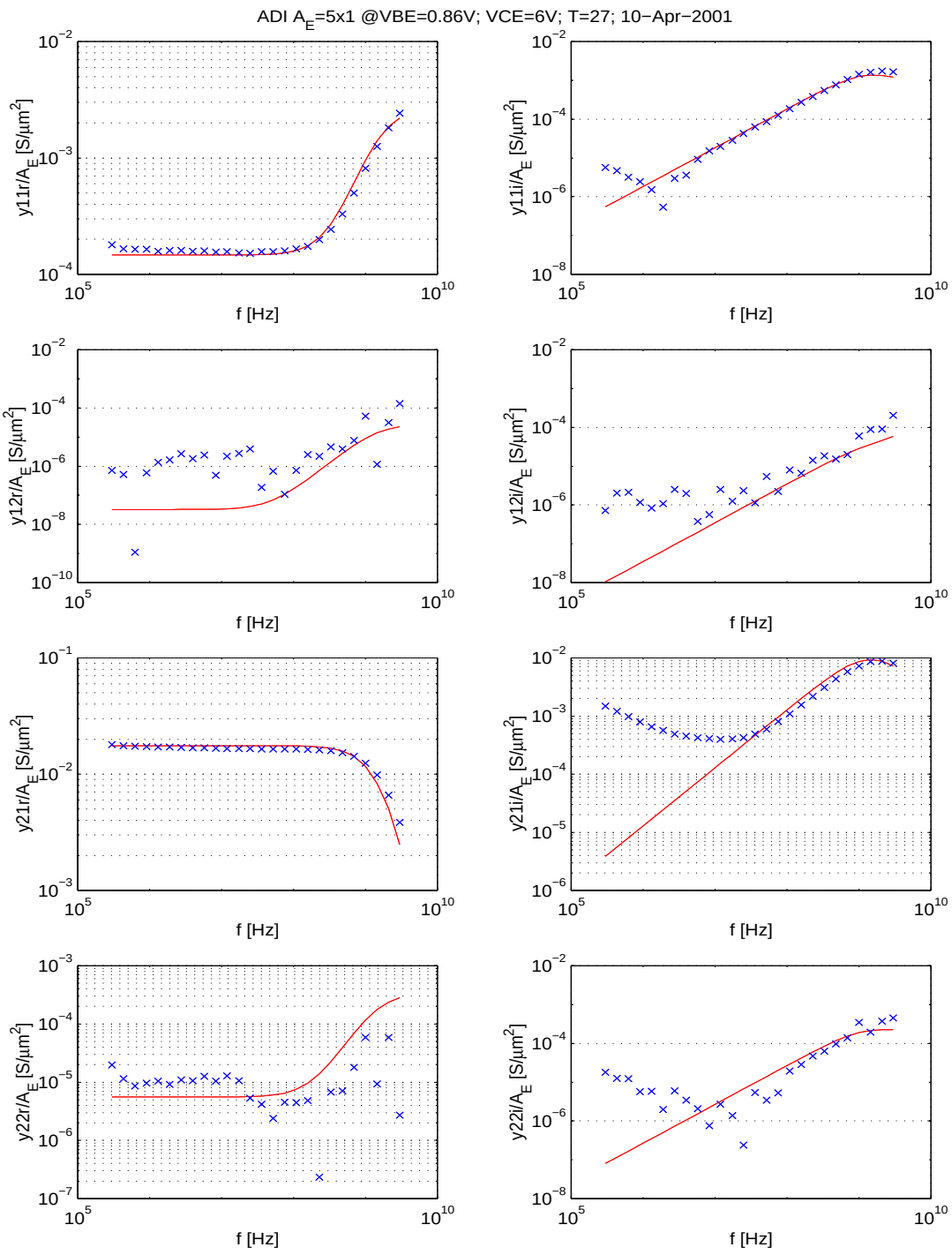

Fig. 1.3/8: Frequency dependent y-parameters at V_{CE} = 6V and I_C/A_E at peak f_T.

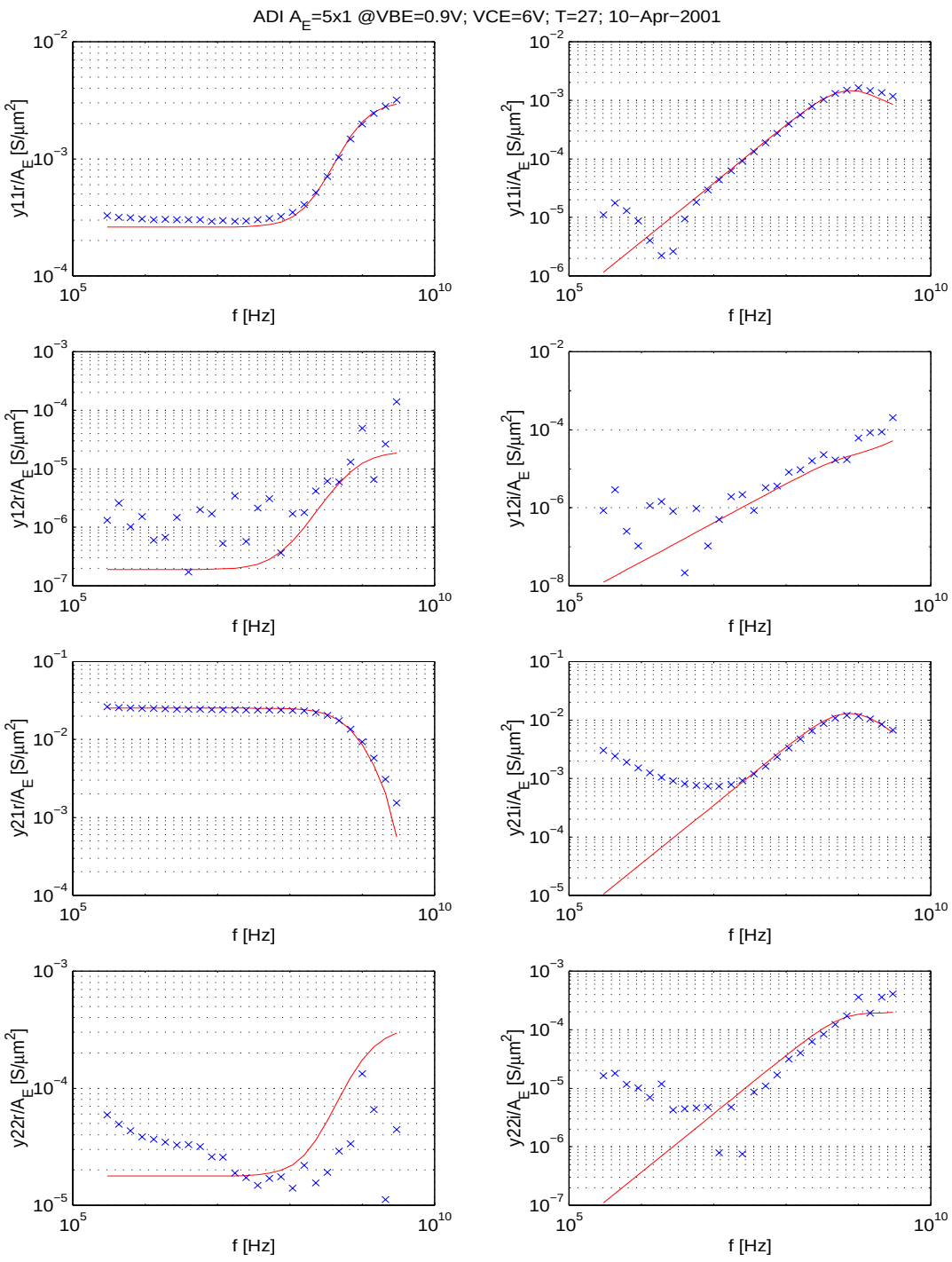

Fig. 1.3/9: Frequency dependent y-parameters at V_{CE} = 6V and I_C/A_E beyond peak f_T.

```
'*'  HICUM / LEVEL2        AC-set
'MODQ' 'Tref' 1
 &HICUM2 c10=3.55E-31     qp0=7.49E-14     ich=6E-03    hfc= 0.5
       hfe= 1.00        hjci= 0.35       hjei= 1.00       alit=0.4
       cjei0=1.49E-14   vdei=0.839       zei=0.309        aljei= 2.0
       cjci0=5.18E-15   vdci=0.505       zci=0.262        vptci=7.00E+00
       t0=16.2E-12      dt0h=1E-18   tbvl=3.200E-12   tef0=0.6E-12
       gtfe=  1.0      thcs=0.85E-10     alhc= 0.25      fthc= 0.5
       alqf=0.2
       rci0=590         vlim= 0.85       vpt=   7.0       vces= 0.080
       tr=5.00E-11
       ibeis=4.70E-20   mbei=1.0100      ireis=1.00E-15   mrei=2.0000
       ibcis=1.00E-30   mbci=1.0980
       favl= 2.65       qavl=2.23E-13
       rbi0= 320.00     fdqr0=0.000      fgeo=0.7300      fqi=0.9050
       fcrbi=0.00
       latb=3.000E+00   latl=0.600
       cjep0=8.93E-15   vdep=0.839       zep=0.309        aljep= 2.5
       ibeps=1.00E-30   mbep=1.0130      ireps=1.00E-30   mrep=2.0000
       ibets=0.00E+00   abet=  0.00
       cjcx0=1.2E-14    vdcx=0.700       zcx=0.700        vptcx=6.0
       ccox=0.00E+00    fbc=0.5
       ibcxs=8.37E-18   mbcx=1.0980
       ceox=0.00E+00    rbx= 110.00      re= 20.5       rcx= 40.00
       itss=1.00E-30    msf=1.000       tsf=0.00E+00
       iscs=1.00E-30    msc=1.000
       cjs0=1.8E-14     vds=4.000        zs=0.15         vpts=1.00E+03
       rsu=1000.0       csu=0.00E+00
       kf=0.00E+00      af=1.00E+00
       vgb= 1.177       alb= 3.94E-03    alt0=0.0   kt0=0.0
       zetaci=  1.30    alvs=1.00E-03    alces=4.00E-04   zetarbi=  0.588
       zetarbx=  0.206  zetarcx=0.223    zetare=-0.425
       alfav=8.25E-05   alqav=5E-03
       rth= 1700.00     cth=0.00E+00  &end
```

Fig. 1.3/10: Set of model parameters for the AC measurement based comparison (DEVICE).

1.4 Results for the “DC” measurement data

Figures 1.4/1 to 1.4/7 contain a comparison between model (solid lines) and measurements (symbols) for T=27C. These “DC” data cover a larger bias range towards *very low* current densities but contain, in contrast to the data from AC measurements, only a subset of V_{BC} values. For the comparison, most model parameters (cf. Fig. 1.4/15) were left unchanged from the previous (“AC”) values, except the ones modeling the various base current components at low current densities and the avalanche current, for which insufficient data was available from “AC” measurements. The forward DC collector current agrees very well with the measurements, while at high current densities (about factor 3 and higher than those at peak f_T) the base current begins to show deviations, the cause of which can be inaccurate series resistances, self-heating or high current effects in I_C which modulate the internal base resistance. As a result, similar deviations occur in the DC current gain. Output characteristics and conductance show good agreement at current densities well beyond peak f_T and start to deviate at *very* high current densities due to uncertainties in the above mentioned parameters and related effects. In general, similar agreement is obtained for the same characteristics that were already compared for the data set from AC measurements. Also, good agreement is obtained for the bias region at very low current densities.

In addition to the usual DC characteristics, several low-frequency derivatives, i.e. (normalized) conductances, are shown.

- In Fig. 1.4/2, the normalized transconductance:

$$\frac{g_m}{I_C} = \frac{1}{I_C}\left.\frac{dI_C}{dV_{BE}}\right|_{V_{BC}}, \tag{1.4.0-1}$$

  Quite good agreement is obtained up to very high current densities.

- In Fig. 1.4/4, the normalized input conductance:

$$\frac{g_{BE}}{I_B} = \frac{1}{I_B}\left.\frac{dI_B}{dV_{BE}}\right|_{V_{BC}}. \tag{1.4.0-2}$$

  The deviations at *very* high current densities can be due to the unknown partitioning of various effects (as already discussed before) and would need further investigation. However, the importance of the above characteristic for circuit design is unclear.

- In Fig. 1.4/7, the output conductance:

$$g_o = \left.\frac{dI_C}{dV_{CE}}\right|_{I_B}. \tag{1.4.0-3}$$

  The agreement is fairly good at low and medium voltages (up to 6V, for which the minority charge data were available from “AC” measurements); at larger voltages, visible deviations occur, which would require further investigation. These deviations are believed mainly to be due to (a) insufficient knowledge about the voltage dependence of the internal BC junction

capacitance (cannot be extracted from a single device) and other relevant parameters, and (b) the weak avalanche model that does not take into account the breakdown mechanism at high current densities (which occurs close to the buried layer).

All derivatives were obtained by numerical differentiation of either the linear (g_o) or log data (g_m, g_{BE}).

As shown in Figs. 1.4/8 - 1.4/14, the temperature dependence of the DC characteristics is modeled well as expected, although only the bandgap and the TC of the current gain were adjusted to the measurement at low current densities. The results at high current densities can be improved by additional measurements from which the TCs of the various resistances and other (transit time, avalanche) parameters can be determined.

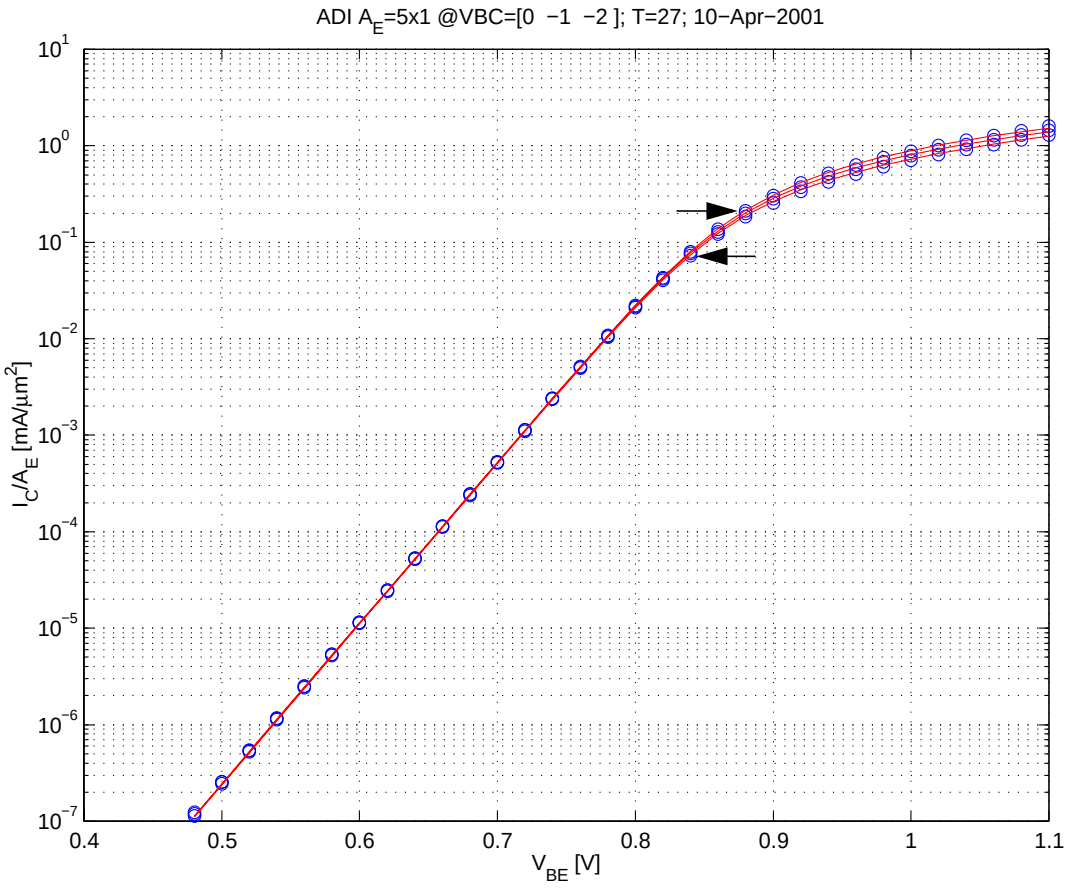

Fig. 1.4/1: Collector current density vs. V_{BE} for V_{BC}/V = 0, -1, -2; T = 27C. Data source: DC measurements.
The arrows indicate peak f_T for the lowest and highest V_{BC} value.

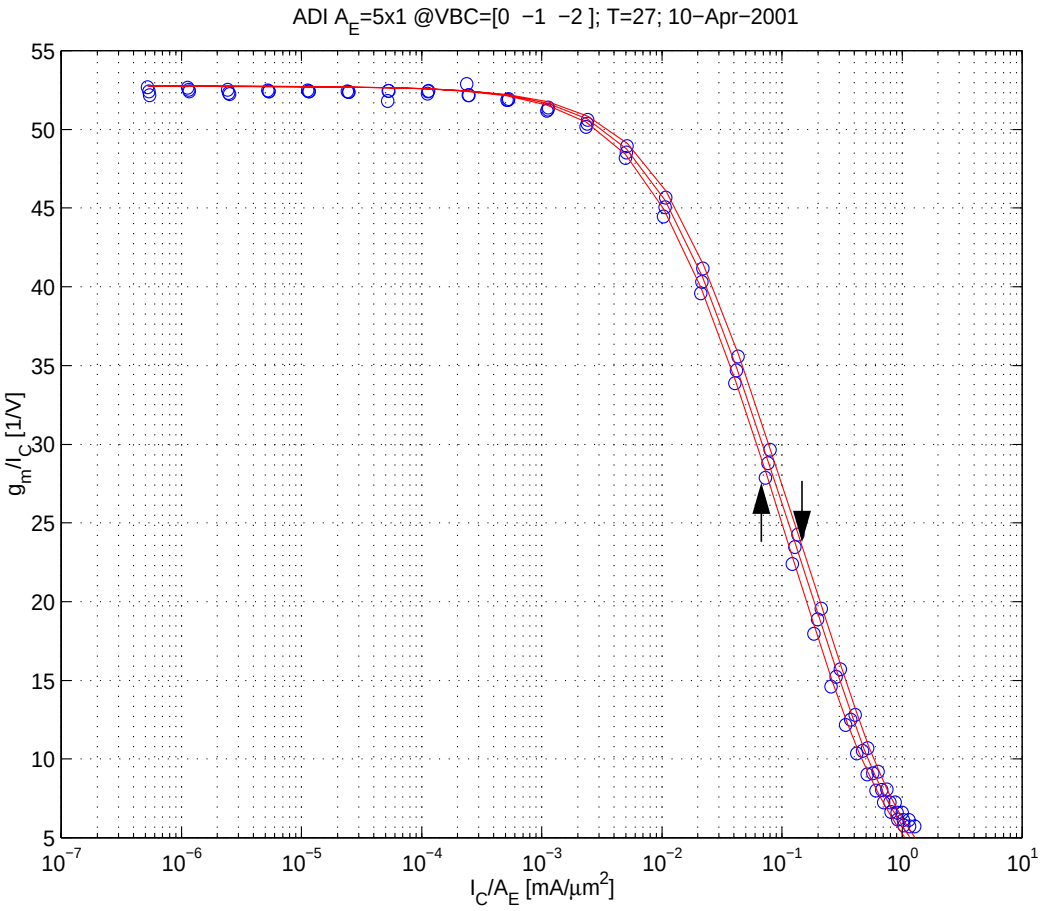

Fig. 1.4/2: Normalized low-frequency transconductance vs. collector current density;
V_{BC}/V = 0, -1, -2; T=27C. Data source: DC measurements.
The arrows indicate peak f_T for the lowest and highest V_{BC} value.

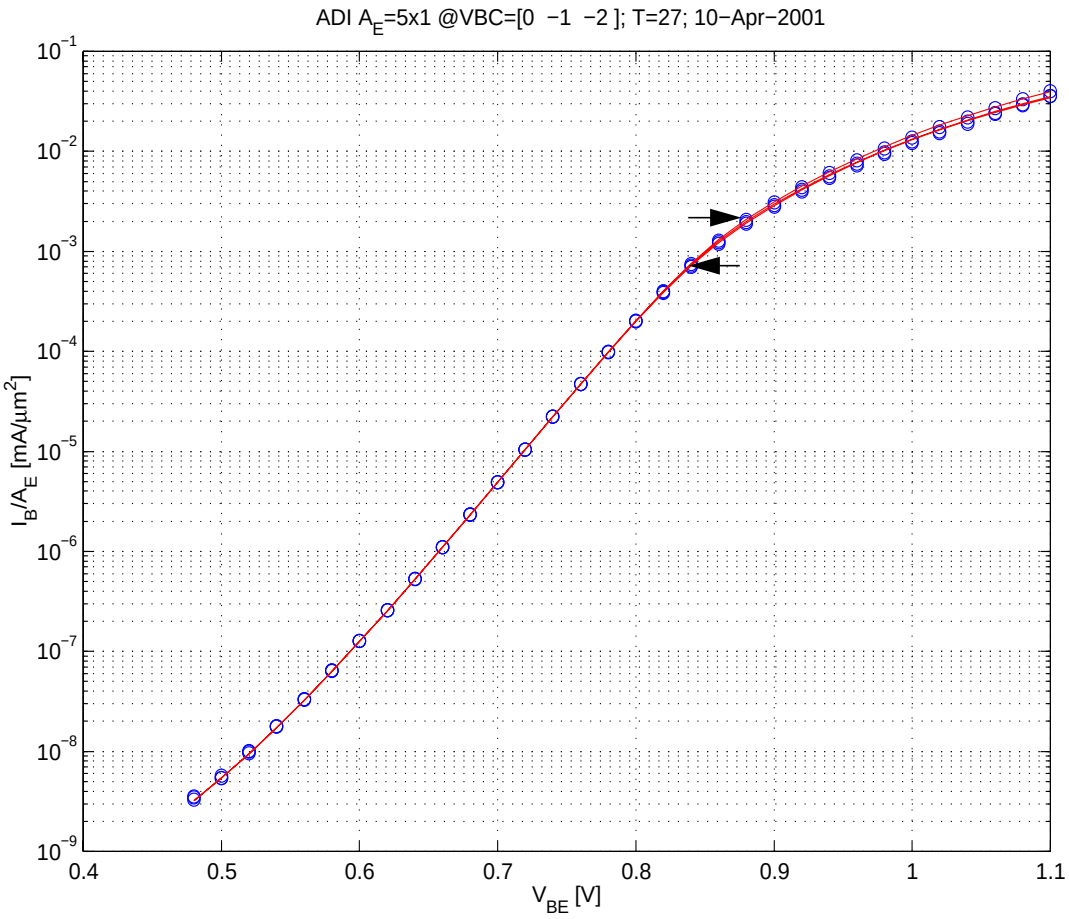

Fig. 1.4/3: Base current density vs. V_{BE} for V_{BC}/V = 0, -1, -2; T = 27C. Data source: DC measurements.
The arrows indicate peak f_T for the lowest and highest V_{CB} value.

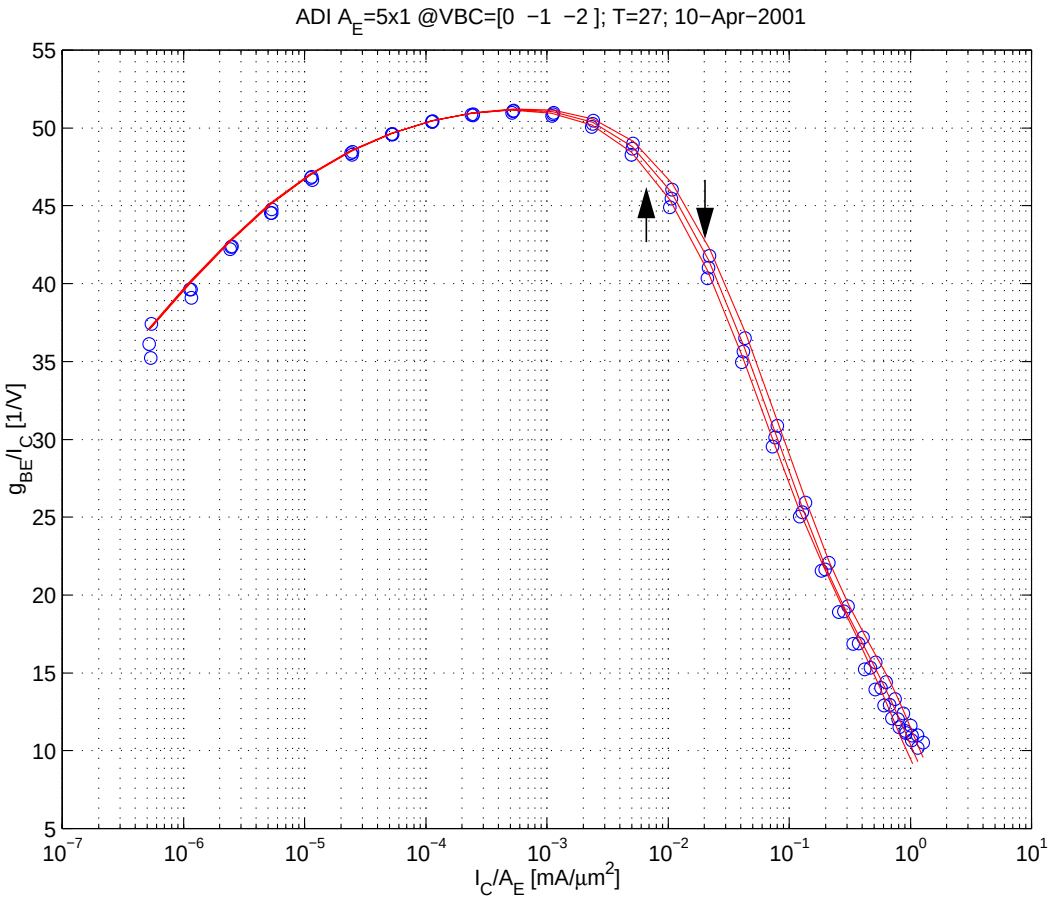

Fig. 1.4/4: Normalized low-frequency input conductance vs. collector current density; V_{BC}/V = 0, -1, -2; T=27C. Data source: DC measurements.
The arrows indicate peak f_T for the lowest and highest V_{CB} value.

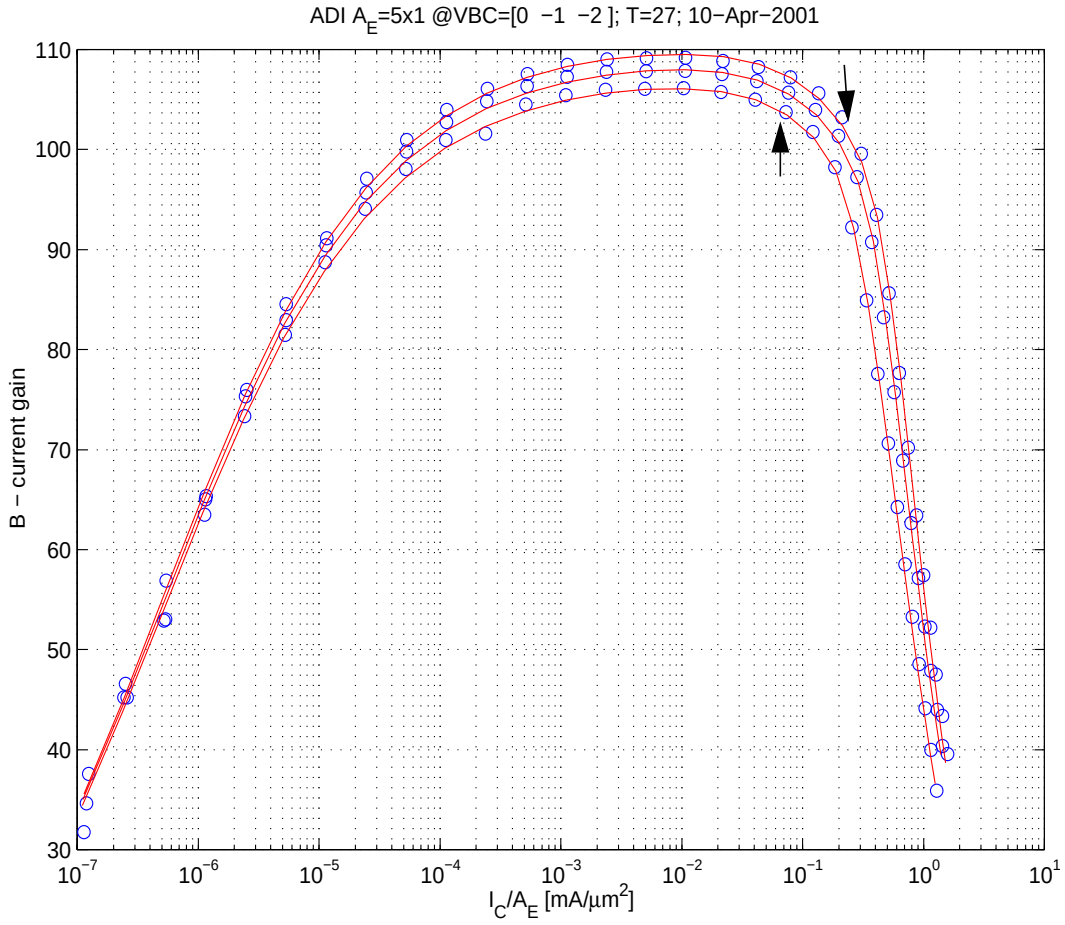

Fig. 1.4/5: DC current gain vs. collector current density for V_{BC}/V = 0, -1, -2; T = 27C. Data source: DC measurements.
The arrows indicate peak f_T for the lowest and highest V_{CB} value.

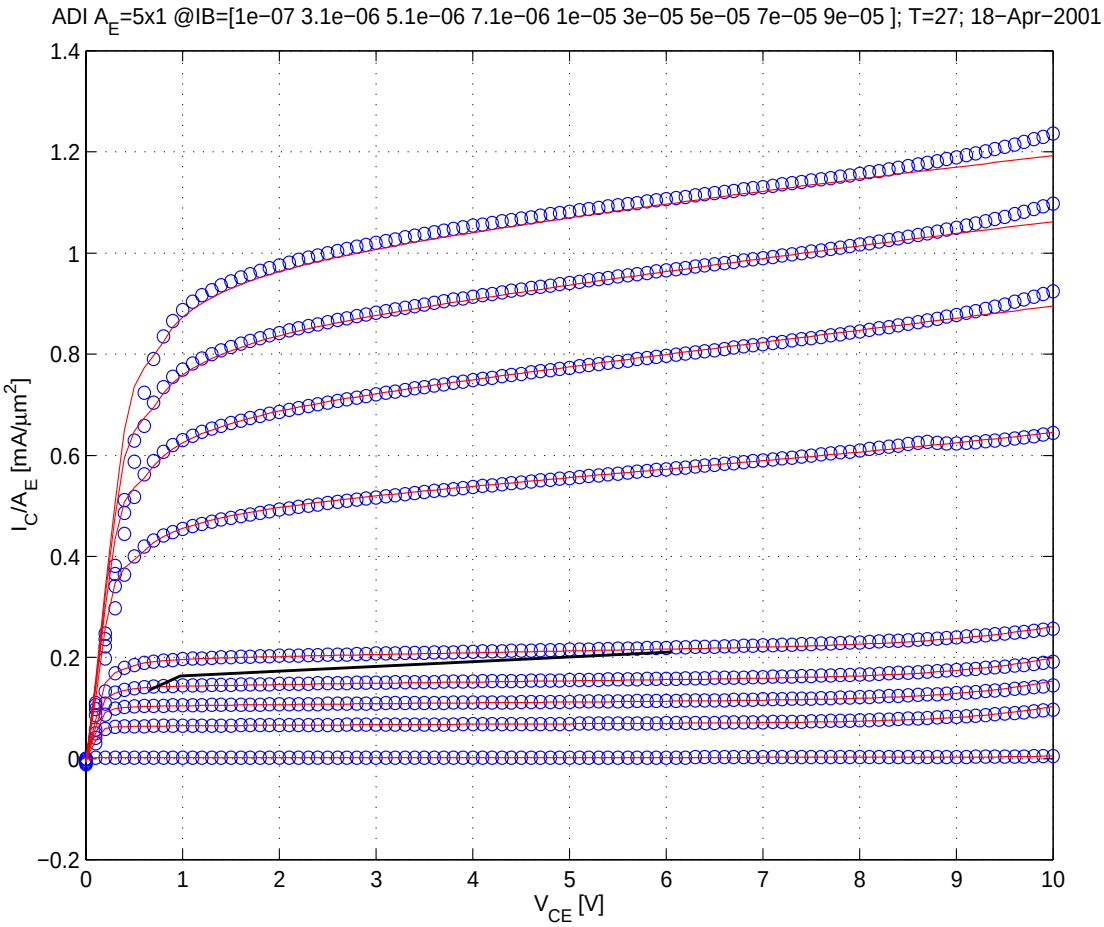

Fig. 1.4/6: Output characteristics for $I_B/\mu A$ = 0.1, 3.1, 5.1, 7.1, 10, 30, 50, 70, 90; T = 27C. Data source: DC measurements.
The bold line indicates the current density at which the peak of f_T occurs.

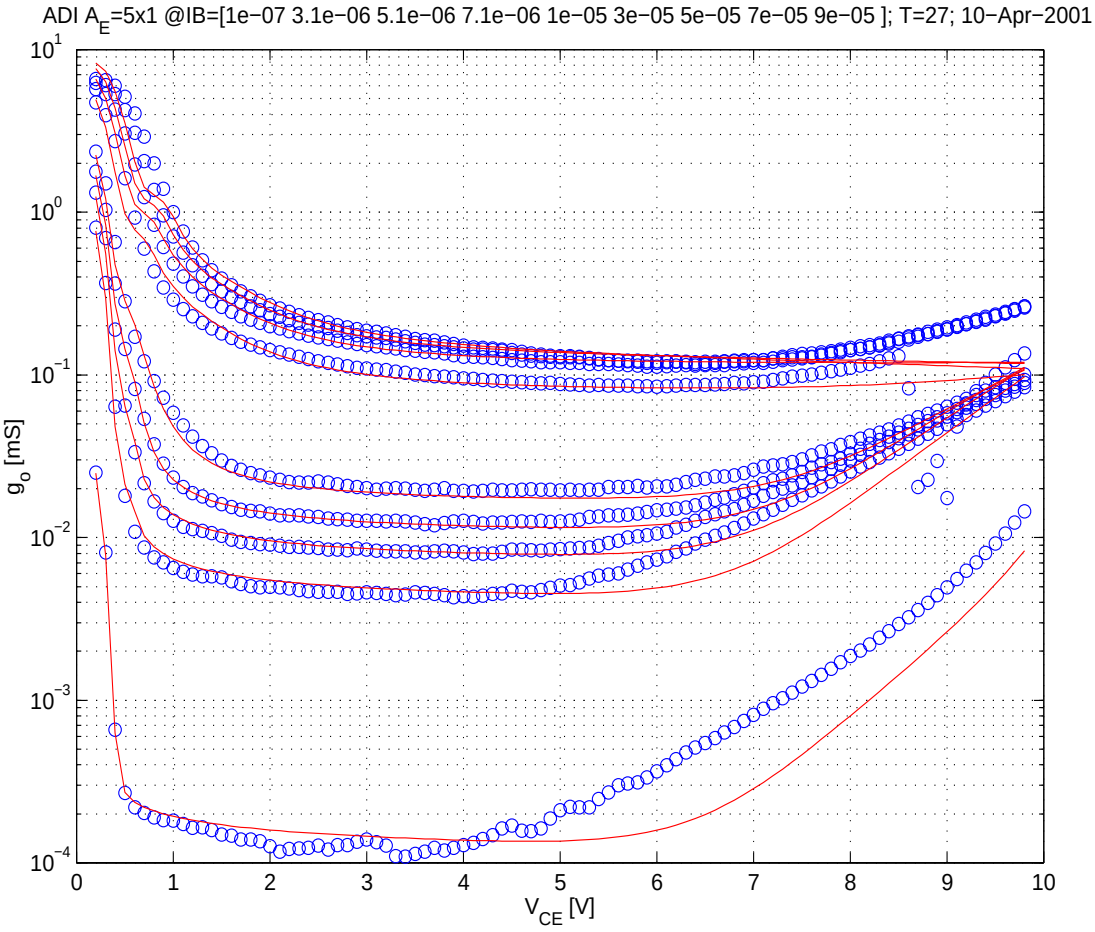

Fig. 1.4/7: Output conductance for $I_B/\mu A$ = 0.1, 3.1, 5.1, 7.1, 10, 30, 50, 70, 90; T = 27C. Data source: DC measurements.

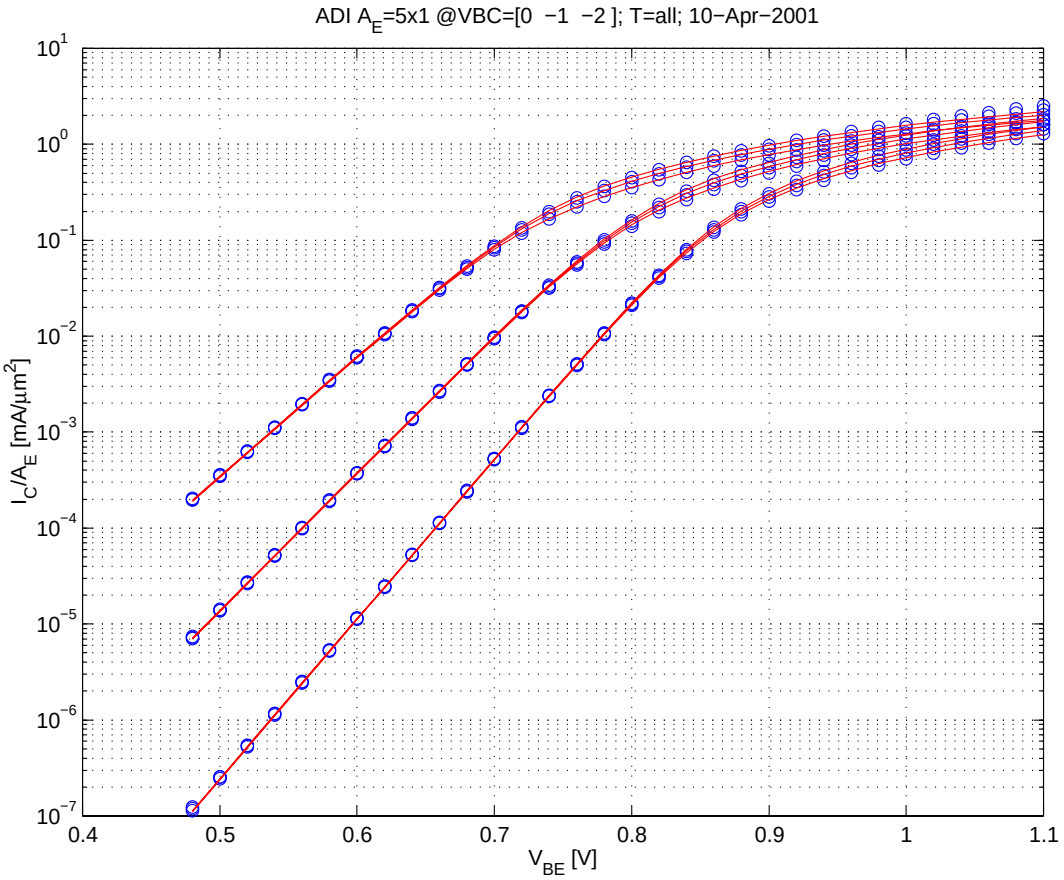

Fig. 1.4/8: Collector current density vs. V_{BE} at different temperatures T/C=27, 75, 125; V_{BC} /V= 0,-1, -2.

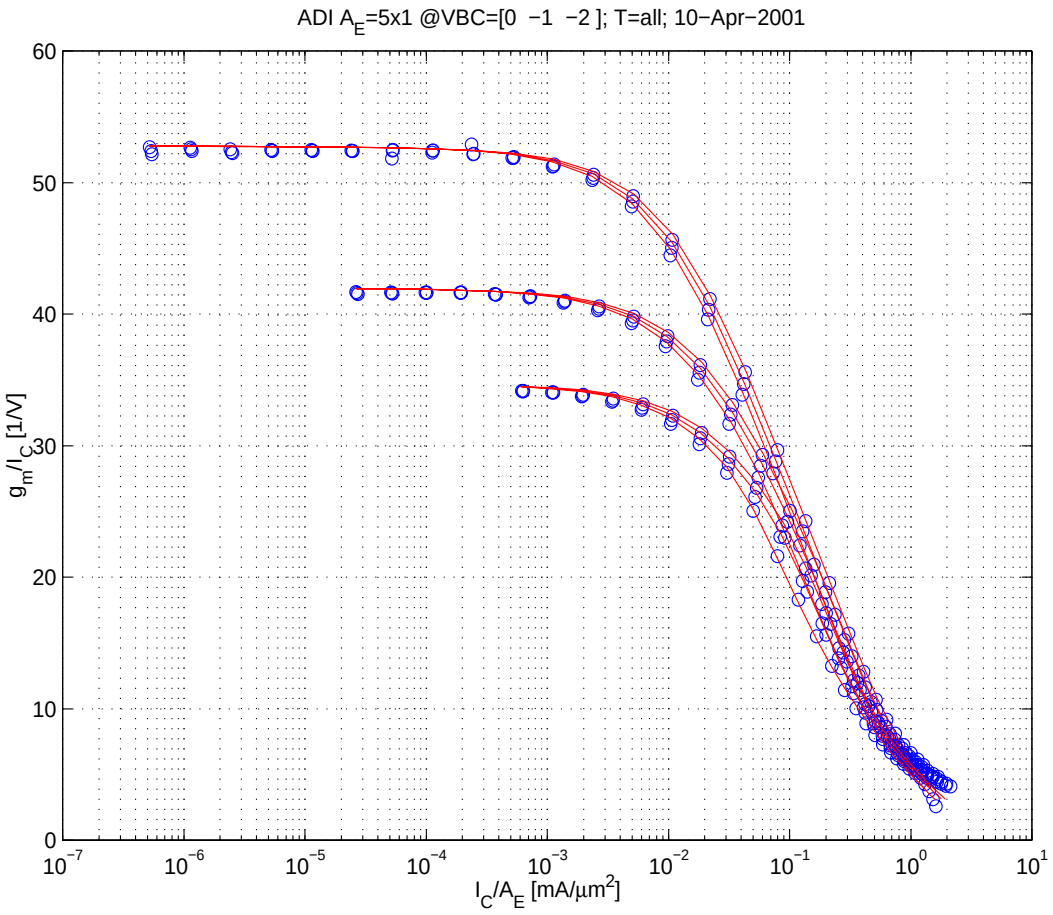

Fig. 1.4/9: Normalized low-frequency transconductance vs. collector current density; at different temperatures T/C= 27, 75, 125; V_{BC}/V = 0, -1, -2.

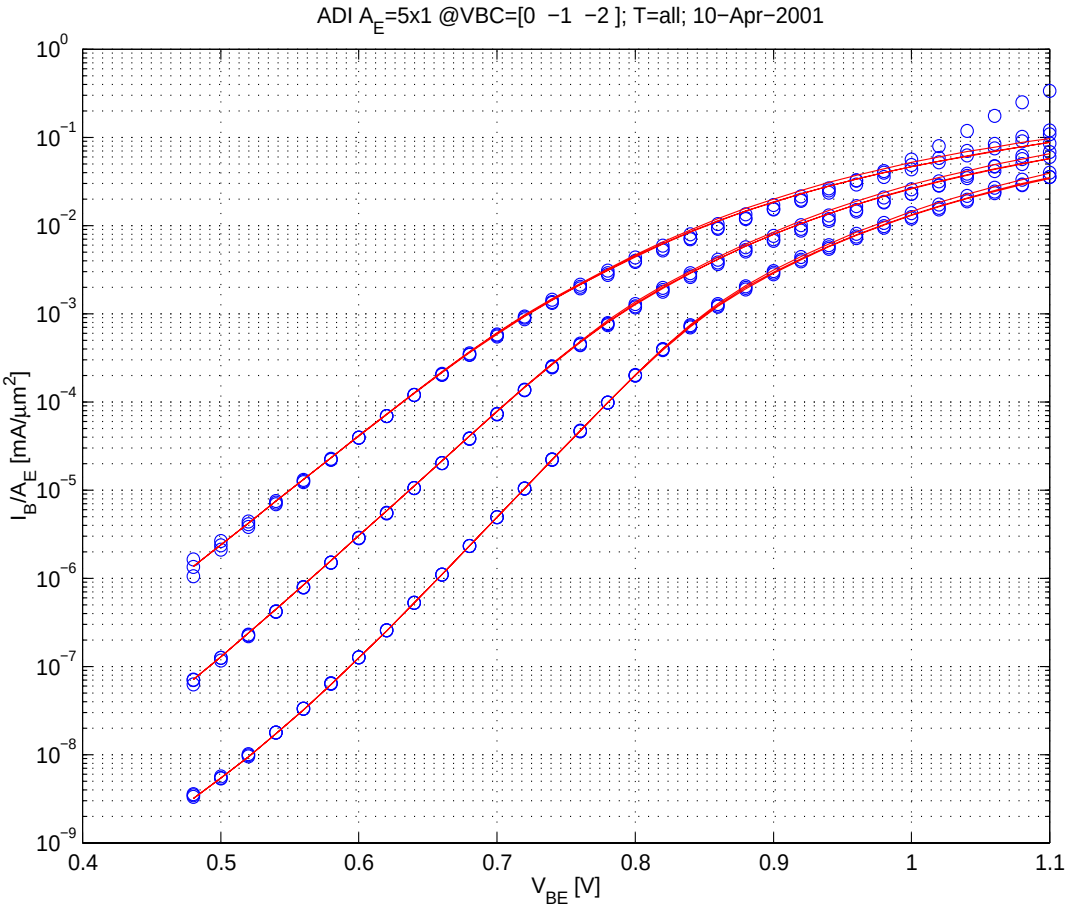

Fig. 1.4/10: Base current density vs. V_{BE} at different temperatures T/C= 27, 75, 125; V_{BC} /V= 0, -1, -2.

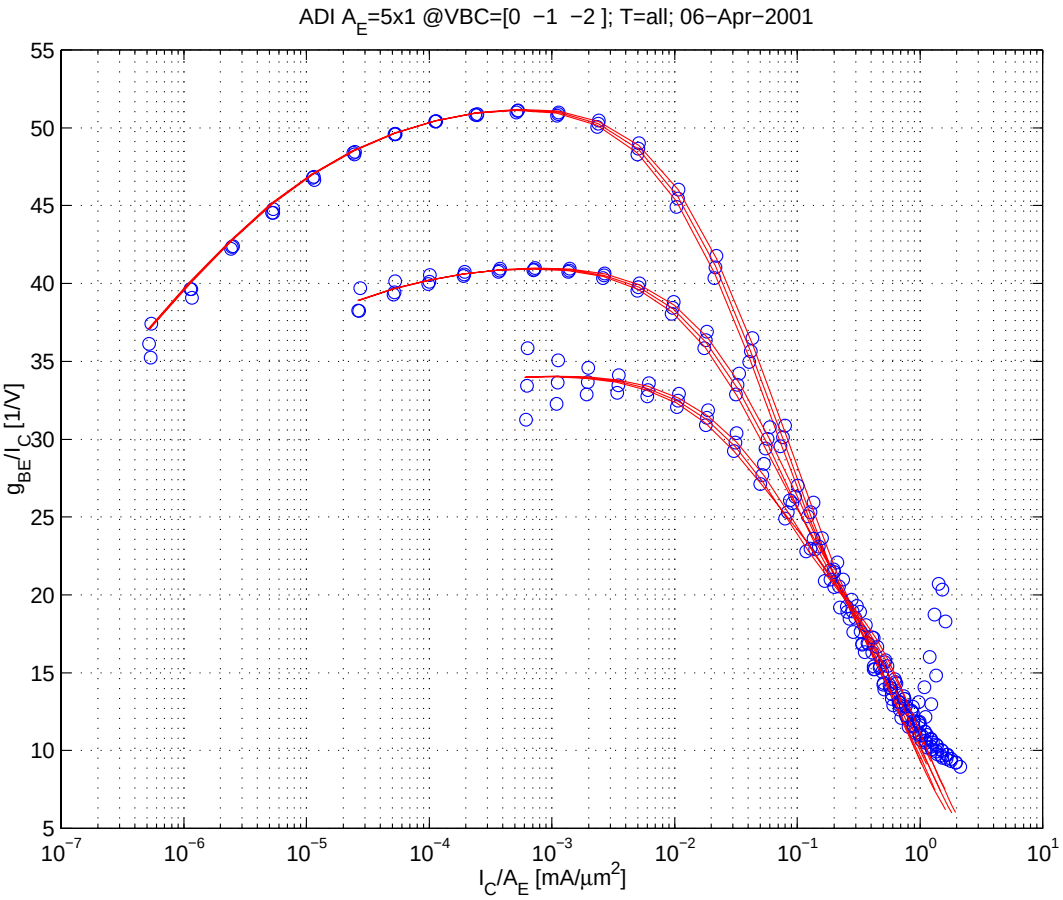

Fig. 1.4/11: Normalized low-frequency input conductance vs. collector current density at different temperatures T/C= 27, 75, 125;
V_{BC}/V = 0, -1, -2; T=27C. Data source: DC measurements.

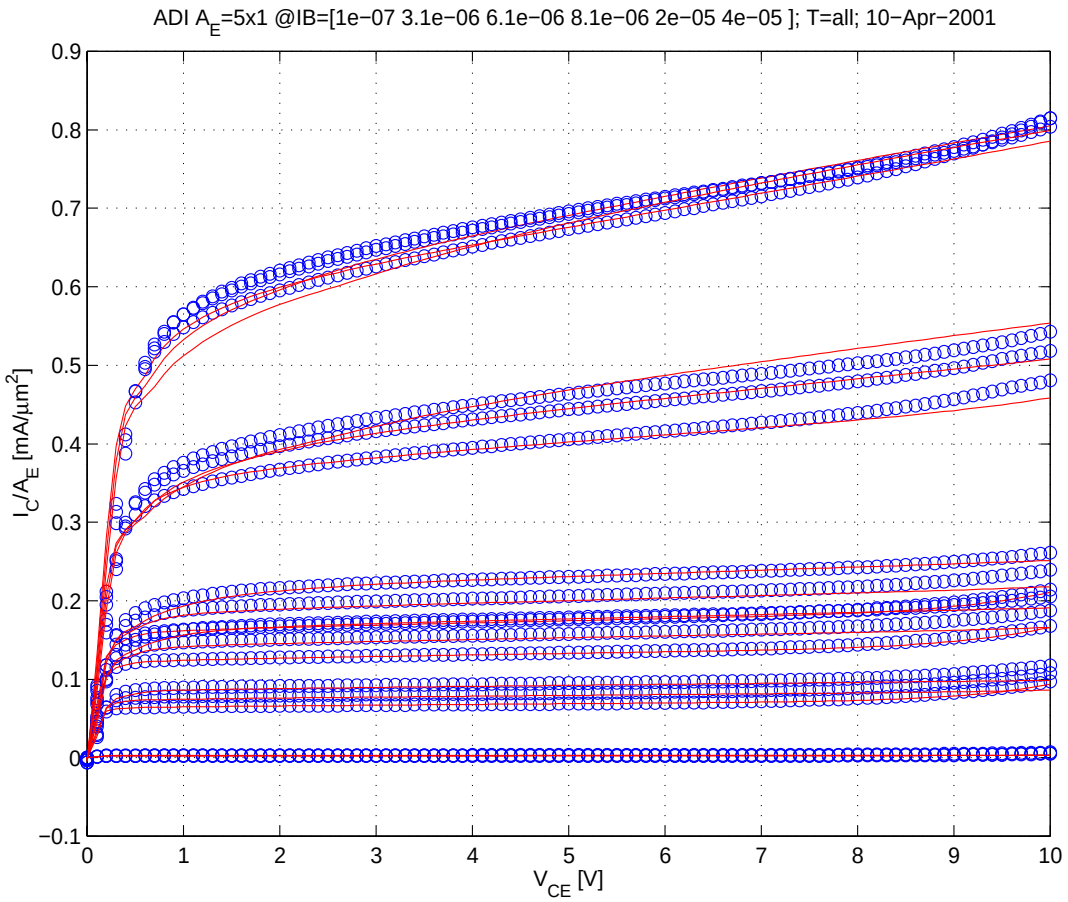

Fig. 1.4/12: Collector current density vs. V_{CE} at different temperatures, T/C= 27, 75, 125; $I_B/\mu A$ = 0.1, 3.1, 5.1, 7.1, 10, 30, 50, 70, 90..

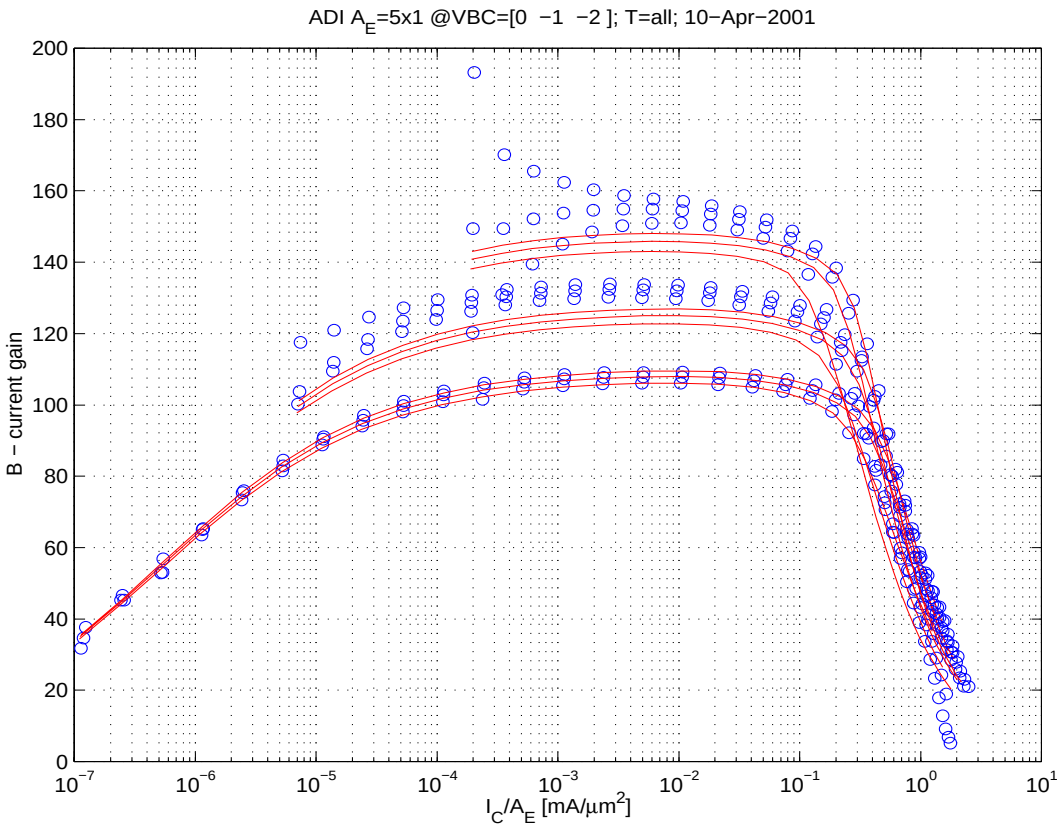

Fig. 1.4/13:DC current gain vs. collector current density for V_{BC}/V = 0, -1, -2; T/C= 27,75,125;. Data source: DC measurements.

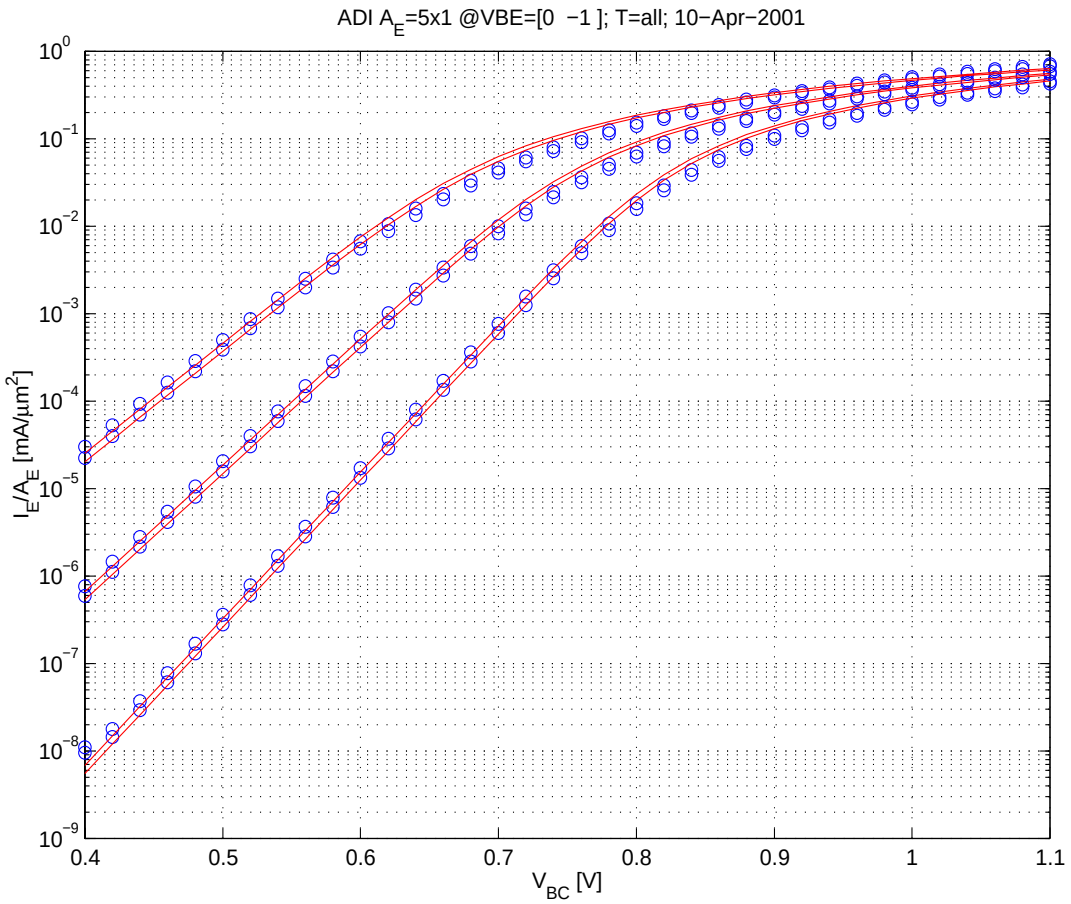

Fig. 1.4/14: Reverse mode, emitter current density vs. V_{BC}
at different temperatures T/C= 27, 75, 125;
V_{BE} /V= 0, -1.

```
'*' HICUM / LEVEL2       DC-set
'*'       cjei0=1.49E-14   vdei=0.839      zei=0.309       aljei= 2.2
'*'       t0=16.2E-12     dt0h=-1.100E-18  tbvl=3.200E-12   tef0=0.6E-12
'*'       gtfe=  1.00      thcs=140E-12     alhc= 0.62      fthc= 1.0
'*'       rci0=520         vlim= 0.7       vpt=   4.30      vces= 0.080
'MODQ' 'Tref' 1
 &HICUM2 c10=4E-31     qp0=7.493E-14     ich=14E-03    hfc=1.3
       hfe= 1.00       hjci= 0.35       hjei= 1.00       alit=0.4
       cjei0=1.69E-14   vdei=0.839      zei=0.309       aljei= 2.0
       cjci0=5.18E-15   vdci=0.505      zci=0.262       vptci=7.00E+00
       t0=16.2E-12     dt0h=1.00E-18   tbvl=3.200E-12   tef0=0.6E-12
       gtfe=  1.0      thcs=1E-10     alhc= 0.25      fthc= 1
       alqf=0.2
       rci0=520         vlim= 0.85       vpt=   7.0       vces= 0.080
       tr=5.00E-11
       ibeis=5.45E-20   mbei=1.0100     ireis=1.00E-15   mrei=2.0000
       ibcis=1.00E-30   mbci=1.0980
       favl= 2.65       qavl=2.15E-13
       rbi0= 320.00     fdqr0=0.000      fgeo=0.7300      fqi=0.9050
       fcrbi=0.00
       latb=3.000E+00   latl=0.600
       cjep0=6.93E-15   vdep=0.839      zep=0.309       aljep= 2.5
       ibeps=1.00E-30   mbep=1.0130     ireps=1.00E-30   mrep=2.0000
       ibets=0.00E+00   abet=  0.00
       cjcx0=1.20E-14   vdcx=0.700      zcx=0.700       vptcx=6.0
       ccox=0.00E+00    fbc=0.500
       ibcxs=8.374E-18   mbcx=1.098
       ceox=0.00E+00    rbx= 110.00      re= 23.5       rcx= 60.00
       itss=1.00E-30    msf=1.000       tsf=0.00E+00
       iscs=1.00E-30    msc=1.000
       cjs0=1.8E-14    vds=4.000       zs=0.150        vpts=1.00E+03
       rsu=1000.0      csu=0.00E+00
       kf=0.00E+00      af=1.00E+00
       vgb= 1.177       alb= 2.9E-03    alt0=0.0   kt0=0.0
       zetaci=  3.4    alvs=1.00E-03    alces=4.00E-04   zetarbi=  0.588
       zetarbx=  0.206  zetarcx=0.223    zetare=-0.625
       alfav=8.25E-05   alqav=5e-3
       rth= 2000.00     cth=0.00E+00  &end
```

Fig. 1.4/15: Model parameter values (DEVICE).